Talanta 102 (2012) 26–33

Contents lists available at SciVerse ScienceDirect

Talanta

journal homepage: www.elsevier.com/locate/talanta

Visual observations of an atmospheric-pressure solution-cathode glow discharge

Andrew J. Schwartz, Steven J. Ray*, Eyal Elish [1], Andrew P. Storey, Arnon A. Rubinshtein [1], George C.-Y. Chan, Kevin P. Pfeuffer, Gary M. Hieftje*

Department of Chemistry, Indiana University, Bloomington, IN 47405, USA

ARTICLE INFO

Article history:
Received 19 July 2012
Received in revised form
30 July 2012
Accepted 31 July 2012
Available online 7 August 2012

Keywords:
Schlieren imaging
Solution cathode glow discharge
Atomic emission spectrometry
Multielement analysis

ABSTRACT

The solution-cathode glow discharge (SCGD) is an optical emission source for atomic spectrometry comprised of a moderate-power atmospheric-pressure DC glow discharge sustained directly upon the surface of an electrically conductive solution. The SCGD boasts a simple, inexpensive design and has demonstrated detection limits similar to those of more conventional excitation sources used in atomic spectrometry. Although the analytical performance of the SCGD as an optical emission source is well characterized, the mechanism through which the discharge atomizes and excites analyte from the sample solution remains a point of debate. The current paper presents visual observations of the SCGD from a variety of imaging techniques. The implications of the images regarding the mechanism of analyte solution-to-plasma transport and excitation in the SCGD are discussed.

1. Introduction

Glow discharges that make use of solution-electrodes have enjoyed increasing interest in recent years, due in part to the number of advantages they offer over other plasma-based sources for the analysis of solution samples. The most prominent alternative is inductively coupled plasma optical emission spectroscopy (ICP-OES), which requires high power (1–2 kW), considerable gas consumption (>15 L min^{-1} Ar) and the sample solution to be nebulized prior to analysis. Solution-electrode discharge systems, in contrast, typically require little or no compressed gas, consume little power (<100 W), and desolvate and excite analyte directly from the sample solution, thereby obviating the need for a sample-solution nebulizer and greatly reducing memory effects. These last attributes make such sources particularly attractive for use with transient sample introduction sources.

A history and detailed description of alternative solution-electrode sources can be found elsewhere [1]. The first solution-electrode system used for elemental analysis, the "electrolyte cathode discharge" (ELCAD), was developed in 1993 by Cserfalvi et al. [2]. In 2005, a simplified design of the ELCAD was introduced by Webb et al. [3], and was given the name "solution-cathode glow discharge" (SCGD) to distinguish it from earlier, somewhat similar sources. Initially, the SCGD and other ELCAD-like sources offered only modest detection limits, ranging from ~10 to 300 ppb [3]. In 2007, a miniature design for the SCGD was described by Webb et al., which achieved detection limits that were comparable to and, in some cases, better than those achievable with ICP-OES [4].

Though the analytical performance and many physical parameters of the SCGD and other sources similar to the ELCAD are well characterized, there remains debate over the mechanisms operative in such sources [1]. Specifically, it is not clear how sample solutions are transported into the discharge and how the resulting droplets are desolvated, vaporized, and atomized and how atoms are finally excited. To date, three possible mechanisms have been proposed to describe the droplet-formation and atomization processes: cathodic sputtering [5–10], thermal desolvation [4], and electrospray [4,11,12].

The first of these proposed mechanisms, cathodic sputtering, is based on the traditionally accepted mechanistic model for a glow discharge source [13]. In this model, positive ions generated in the negative glow are accelerated toward the discharge cathode (in this case the sample solution), which is held at a lower potential than the anode of the source. When these ions collide with the solution cathode they cause atoms, or in the case of the SCGD, solution droplets, to sputter from the cathode surface. The freed droplets can then undergo atomization and excitation in the discharge.

Cserfalvi and Mezei [6] suggested a mechanism for how sputtering could occur in ELCAD-like sources, based on ICP-OES studies using an ELCAD as a nebulization device. In this mechanism, a droplet ejected from the solution-cathode surface by sputtering is desolvated by being passed through a series of four mass-transport zones in the discharge. Each of the four mass-transport zones acts

* Corresponding authors. Tel.: +1 812 855 2189; fax: +1 812 855 0958.
E-mail addresses: sjray@indiana.edu (S.J. Ray), hieftje@indiana.edu (G.M. Hieftje).
[1] Permanent Address: Nuclear Research Center, Be'er-Sheva 84190, Israel.

0039-9140/$ - see front matter © 2012 Elsevier B.V. All rights reserved.
http://dx.doi.org/10.1016/j.talanta.2012.07.096

upon the sputtered droplet in a different way, namely desolvation, charge stripping, bond breaking, and atomization, sometimes ending in the generation of a free atom of analyte.

Makismov et al. [7] proposed an alternative mechanism for the generation of analyte atoms from sputtered material in ELCAD-like sources. This mechanism is rooted in the generally accepted paradigm that salts in aqueous solutions exist as solvated ions. Makismov et al. hypothesized that these solvated ions are ejected into the discharge via sputtering of water clusters from the solution cathode. In the discharge, the ions are excited to high vibrational energy levels, at which the potential energy curves for the ionic form and covalent form of given salts typically cross over. The vibrationally excited ionic salts transition from ionic states to covalent states at these high vibrational levels and dissociate as neutral atoms in the discharge.

Another mechanism, thermal desolvation, was offered by Webb et al. [4] and is based on spatial temperature maps collected for the SCGD source [3]. The temperature profiles indicate that the SCGD is hottest at the solution surface (with Fe excitation temperatures of ~5000 K and gas-kinetic temperatures reaching ~3500 K) [3]. They hypothesized that such a high temperature would be capable of violently vaporizing the analyte solution at the cathode surface, thermally desolvating and exciting the analyte atoms within the solution [4]. However, Webb et. al. also cautioned that this mechanism seems unlikely because many elements emit within a millimeter of the cathode surface of the SCGD, and that thermal vaporization would be unlikely to achieve efficient desolvation and excitation of analyte atoms so close to the cathode surface [4].

Finally, electrospray liquid free-jet formation on the solution surface has also been put forth as a possible mechanism [4]. This mechanism is based on the fact that the analyte solution is subject to the electric field generated by the SCGD plasma. If this electric field were to exceed $\sim 2.7 \times 10^6\ V\ m^{-1}$ (the voltage required to electrospray a perfectly flat, pure water–air interface) [14], then it likely that analyte species could be electrosprayed from the solution surface within the SCGD. Cserfalvi and Mezei have measured the cathode fall of an ELCAD cell to be 515 V [5], and have estimated the electric field in the cathode-fall region of the ELCAD to be on the order of $1 \times 10^7\ V\ m^{-1}$ [6]. Similarly, Bruggeman estimates the cathodic electric field in a similar system to approach $6 \times 10^6\ V\ m^{-1}$ [11,12]. It is plausible then that electrospray could account for a large portion of the atomization process in the SCGD.

Clearly, the mechanism of solution-to-plasma transport in SCGD-like sources is still not well understood, and solution-transport mechanisms that have been offered are largely hypothetical and not well supported by experimental data. Because determining this mechanism could help in further optimization of the SCGD source, boosting its analytical performance, it is clear that more research on this topic is merited. The present study provides guidelines regarding the mechanism of atom formation in the SCGD by observations made with a variety of imaging techniques. These techniques included high-speed video photography of the ignition sequence of the source, laser-scattering imaging, and broadband as well as monochromatic imaging at framing times from 100 ns to 100 μs. The implications of the observations made from each of the imaging techniques on the mechanism of solution-to-plasma transport in the SCGD are discussed.

2. Experimental

2.1. SCGD cell design

Shown in Fig. 1 is a diagrammatic representation of the SCGD cell used in this research. In this design, sample solution was

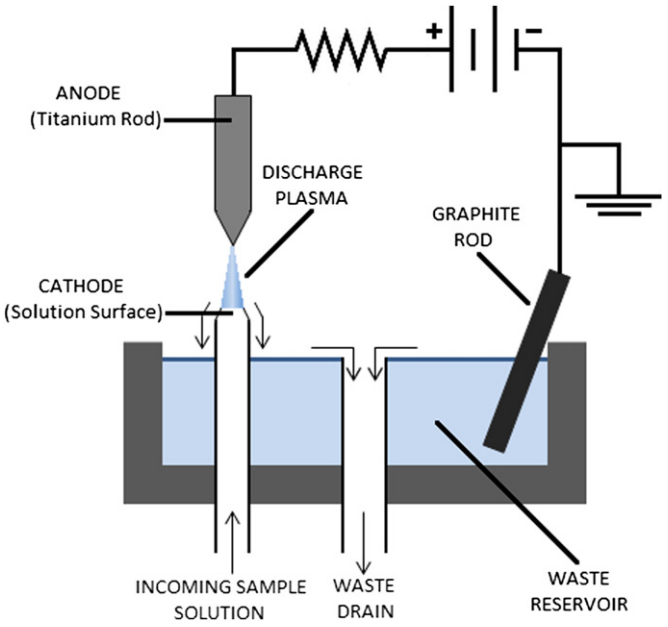

Fig. 1. Schematic diagram of the SCGD cell.

pumped into the cell via a peristaltic pump through a glass capillary with an internal diameter of 0.5 mm and external diameter of 6.5 mm. This capillary was oriented vertically in the SCGD, and above it a 3.25 mm diameter titanium rod served as the anode for the discharge. Both the tip of the pipette and the anode were ground down to create a pointed structure at their ends (tip angles of 30° and 45° respectively), which results in the discharge being more spatially stable. A positive potential was applied to the titanium anode through a current limiting 1.25 kΩ ballast resistor from a high-voltage DC power supply (Universal Voltronics, Brookfield, CT, Model DDC-5-400 R). The sample solution overflowed from the capillary tip into a 60-mL Teflon® waste reservoir, and was grounded via a graphite electrode. The overflow in the cell served to create an electrical connection between the incoming sample solution at the capillary tip and the grounded solution in the waste reservoir. In order to ignite the discharge, the titanium anode was brought near to (<1 mm) the sample-solution surface by means of a micrometer stage at the same time a high potential (≥ 750 V) was applied. A glass pipette was positioned vertically in the waste reservoir and served to draw waste solution away at the same rate the sample solution entered the cell, maintaining a constant solution level in the waste reservoir.

2.2. High-speed videography of the SCGD ignition sequence

High-speed videos of the effects of SCGD ignition on the cathode solution were obtained through the use of a Casio Exilim Ex-F1 camera (Tokyo, Japan), which recorded video at a rate of 1200 FPS. The camera was mounted on the objective lens of a stereomicroscope (Bausch and Lomb, Rochester, NY, Model 1955-RR-513) that viewed the SCD side-on during the ignition sequence.

2.3. Laser-scattering images of the SCGD

A diode laser controller (Melles Griot, Albuquerque, NM, Model 06DLD103) was used to power a diode laser (Sony, New York, NY, Model SLD1239JL-54) that produced a 100 mW 658 nm incident beam. The diode laser was directed through the solution–plasma interface of the SCGD and Mie-scattered radiation was viewed with a stereomicroscope (Edmund Industrial Optics, Barrington, NJ, Model NT52-352) positioned at an angle of 10–15° from the

incident laser beam. Images were collected with a Canon EOS Digital Rebel XT Camera (Lake Success, NY) affixed to the stereomicroscope via a C-T mount.

2.4. Broadband and monochromatic imaging of the SCGD

Broadband images of the SCGD were obtained at framing at speeds of 100 ns–100 μs through the use of an intensified charge coupled device (ICCD) camera (Roper Scientific, Trenton, NJ, Model 7361-0017). The ICCD camera was positioned at an angle of 30° from the solution surface of SCGD and the image was focused via a Nikon AF NIKKOR 50 mm, 1:1.8 camera lens. Image analysis was conducted by means of ImageJ (NIH, Bethesda, MD).

Monochromatic images of the SCGD were collected at framing speeds of 100 ns–100 μs with the same ICCD camera and a monochromatic imaging spectrometer (MIS) of the kind described by Olesik and Hieftje [15]. The SCGD source was positioned at the focal distance of a 50 mm focal length plano-convex quartz collimating lens. The resulting collimated light was directed onto the entrance slit of a Heath (Model EU-700) 0.35 m Czerny-Turner monochromator outfitted with a grating of 1200 lines mm^{-1} spacing. Upon exiting the monochromator, the collimated light was directed onto a 100 mm focal length plano-convex quartz lens, which refocused light onto the ICCD camera with a magnification factor of 2.

3. Results and discussion

3.1. High-speed video of the SCGD ignition sequence

Selected images captured from a high-speed video of the ignition of the SCGD atop an incoming 0.1 M HNO_3 sample solution flowing at the rate of 3.0 mL min^{-1} are shown in Fig. 2 (the entire video is available as electronic supplementary information [ESI] Videos 1 and 2). In this instance, the discharge was ignited by reducing the distance between the anode tip and the solution surface by means of a translational stage, allowing the proximity of the anode (held at +900 V) and the cathodic solution to initiate electrical breakdown and plasma formation. After ignition, the anode was returned to its position 3 mm above the surface of the solution and the +900 V was sustained across the discharge. The images shown in Fig. 2 represent the first moments of plasma stabilization. In Fig. 2, frame 2, the anode tip and cathode solution are separated by approximately 290 μm, but no breakdown has yet occurred. Captured 86 ms later, the next frame depicts the plasma already in place, and subsequent frames follow stabilization of the discharge. The discharge voltage and current monitored during the ignition event indicate that the SCGD plasma reaches a steady-state electrical condition after approximately 30–90 ms (see ESI information). Thus, frames 2–6 are indicative of a plasma structure similar to the equilibrium condition. Similarly, frames in the video sequence following frame 6 show essentially identical physical structure. When the distance between the anode and cathodic solution was increased from 0.9 mm as shown in Fig. 2 to the typical operating distance of 3 mm, the SCGD retained the same physical structure.

Supplementary material related to this article can be found online at http://dx.doi.org/10.1016/j.talanta.2012.07.096.

Several observations can be made from the sequence of images in Fig. 2. Most importantly, SCGD ignition causes the normally convex surface of the liquid atop the delivery capillary to deform toward a concave shape and retreat from the anode, eventually forming a flat cathode surface when the discharge has reached equilibrium. The familiar positive surface contact angle of the analyte solution overflowing from the end of the glass introduction capillary (e.g. Fig. 2, frame 2) reflects the surface tension of the aqueous nitric acid solution (approximately 72.1 mN m) [16]. In the early stages of ignition, however, the portion of the liquid surface in contact with the discharge shows a marked shape change (Fig. 2, frame 3) until the observed contact angle is approximately 0 degrees in Fig. 2, frame 6. The change in liquid meniscus could reflect the influence of several phenomenon. The deformation could simply be the result of rapid vaporization of the solution, causing a local concave deformation due to the loss of solution to the vapor phase. Prior work from this group has determined the gas-kinetic temperature of the plasma in the region immediately above the solution surface to be >3000 K [3], a value similar to that reported by others [11,17]. Such a high gas temperature in close proximity with the condensed phase liquid could result in flash evaporation of the solution. However, it would seem unlikely that this mechanism alone is responsible for the difference in surface shape, since this would require that the mass loss through vaporization would have to balance the mass provided by the solution constantly replenishing the liquid surface. The difference in density between water vapor and liquid ($\sim$1250-times) would also create a significant cloud of water vapor, and only minute amounts of steam are observed. Further, the SCGD is also known to operate over a range of solution flow rates, cathode capillary sizes, and solution types showing only very slight, if any, change to the physical structure shown in Fig. 2. Nevertheless, it is also possible that heated gases and water vapor in the core of the discharge could create a slight overpressure above the surface of the solution. This overpressure could contribute to the observed deformation.

Alternatively, the deformation of the solution surface could reflect a change in surface tension or composition, leading to the near-zero contact angle observed during SCGD operation, as indicated by the convergence of the liquid–vapor and liquid–solid interfaces, shown in Fig. 2, frame 7. Several factors can affect liquid surface tension; however, the high electric field at the solution–plasma interface is the most likely cause. Prior work in this laboratory, and others, has shown that the SCGD exhibits a spatially distinct series of plasma regions common to glow discharges [3,18]. Each region within the discharge possesses a characteristic electric field and ion density that depend upon the

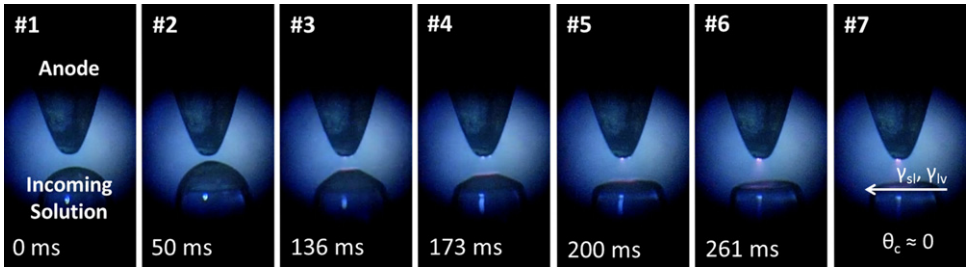

Fig. 2. Images taken from high-speed video of the SCGD ignition process. Note the change in the meniscus of the flowing 0.1 M HNO_3 solution as the discharge ignites, arriving at a contact angle (θ_c) of approximately zero, as indicated in frame seven.

mechanism dominant at that location. The interface between the negative glow of the SCGD and the liquid surface includes the cathode fall of the glow discharge, which is the spatial portion of the discharge where most of the electric potential is dropped. In this zone, positive gaseous ions are accelerated towards the cathode surface without collision with the background gas, permitting the ions to achieve high velocities (and therefore energies) before impacting the cathode surface. This is the mechanism by which cathodic sputtering operates. Because the SCGD operates at atmospheric pressure, however, the mean-free path requires that the cathode-fall region be thin (on the order of several micrometers). Because of this, a voltage of several hundred volts applied across such a small dimension would create a very significant local electric field. In turn, the high electric field would reduce the surface tension.

The potential developed across the cathode-fall portion of the SCGD discharge was estimated in a separate experiment by using the method of Cservalfi et al. [5,11]. Here, the dependence of discharge current on applied voltage was monitored at several different separation distances between the metallic anode and the cathodic solution of the SCGD. In this analysis, it is assumed that the thickness of the cathode-fall region of the SCGD will be unaffected by the interspacing of anode and cathode. Thus, increasing the distance between anode and cathode will raise the impedance of the discharge in an additive manner. A plot of several *i*–*V* curves collected at different inter-electrode distances will then show different slopes, but a common *y*-intercept equal to the cathode drop (such a plot is included in the ESI). From this technique, a cathode-fall potential of 736 ± 2 V was measured for the discharge depicted in Fig. 2. The physical length of the cathode fall is much more difficult to ascertain, but could be on the order of the mean-free path of the local environment. Cservalfi et al. have estimated the distance to be larger in the ELCAD, on the order of 100 μm [5,19], and Bruggeman et al. have estimated similar distances [11]. Even with this conservative estimate of cathode-fall length, the calculated electric field at the plasma–liquid interface is 7.4×10^6 V m^{-1}. Such a high electric field at a liquid solution surface is certainly sufficient to alter the surface free energy (surface tension), and to cause local instability of the liquid and the formation of liquid free-jets [14,20].

The pressure exerted by the cathodic sputtering action could itself contribute to the change in meniscus shape. Ions accelerated through the cathode-fall achieve high energies before striking the solution, exerting a force on the liquid surface that could lead to its deformation. The force acting on a surface due to ion bombardment can be calculated as

$$F = \frac{I}{e}\sqrt{2meV} \quad (1)$$

where e is the fundamental charge, I is the ion current striking the surface, m is the mass of the bombarding ion, and V is the acceleration potential of the ion [21]. Mezei and coworkers have estimated that the terminal energy of an ion striking the solution surface of the ELCAD to be 90 eV [5,19]. Assuming the main bombarding ion to be molecular nitrogen, an ion current of 100 mA accelerated to 90 V over the cathode fall before striking the solution surface would exert a force of 0.72 mN; ions experiencing the entire cathode fall potential of 700 V would exert a force of 2 mN upon the surface. This relatively weak force seems unlikely to be of very great importance overall.

The sequence of later images in Fig. 2 also illustrates the transient and spatially heterogeneous nature of the SCGD interface with the liquid surface. While the liquid surface maintains a more-or-less constant level and surface structure, the discharge shows dynamic motion with areas of higher-intensity at different points along the liquid surface. Further, the luminous portions of the SCGD discharge anchor atop the cathodic solution and appear to cover only a portion of the available surface area.

3.2. Laser-scattering images

In order to better characterize the plasma–solution interface, the solution–plasma interface of the SCGD was visualized under optical magnification by means of the previously described laser-scattering setup. A solution flow rate of 3.4 mL min^{-1} of 0.1 M HNO_3 sustained the discharge, which was operated at an applied power of 72 W (900 V and 80 mA). A representative image is included as Fig. 3(a), and a video of this process obtained with similar conditions is available as ESI. Light scattered from an incoming laser beam (635 nm) was observed at a low angle (~10 degrees) to reveal both scattering from droplets or particles within the plasma and to illuminate the liquid surface. In Fig. 3(a), the ejection of droplets or particles from the solution surface during the 12.5 ms exposure creates traces of scattered radiation that mark the path of their flight. It is clear that the SCGD solution surface is violently chaotic, with a great deal of droplet ejection and solution aerosol formation. The pale blue emission atop the solution surface in Fig. 3(a) is indicative of the cathode-fall and negative-glow region of the glow discharge, where much of the atomic emission occurs and where the electric field is the greatest. In this region, the origin of the droplets is often marked by a bright point of scattered radiation with droplet tracks moving from the solution surface upwards towards the positive column of the SCGD. Interestingly, in some instances the tracks from ejected droplets broaden and disperse as they move away from the solution surface. The broadening of the tracks might indicate droplet fission or evaporation, and the plume-like shape is also similar to the Taylor-cone structure observed with cone-jet electrospray [14,20,22]. The presence of solution droplets being ejected from the surface provides evidence against a purely thermal mechanism of desolvation, as such a mechanism would generate mainly solution vapor and not discrete droplets.

Past work has shown that analyte emission from the SCGD declines as the pH of the analyte solution is increased [2,3,7]; accordingly, one set of experiments studied the effect of solution pH upon surface droplet generation by means of a series of solutions of different acid concentration but with constant ionic strength. The prepared solutions were 100 mM HNO_3, 25 mM KCl in 75 mM HNO_3, 50 mM KCl in 50 mM HNO_3, 75 mM KCl in 25 mM HNO_3, 90 mM KCl in 10 mM HNO_3, 95 mM KCl in 5 mM HNO_3, 97.5 mM KCl in 2.5 mM HNO_3, and 100 mM KCl. The secondary electrolyte was chosen to be KCl, as its most intense atomic emission line (at 766.4 nm) lies outside the visible region of the spectrum and would thus not appear in the collected images. Laser-scattering images of each solution were collected at a constant applied discharge power of ~80 W (990 V, 80 mA).

A representative series of images collected in this study can be found in Fig. 3(b), (c) and (d). These images reveal that as the concentration of acid in the solutions was reduced, there was a noticeable decline in the formation of solution aerosol and ejected droplets. This change is particularly apparent in the transition between the images of Fig. 3(b) and (c) collected with solutions of 25 mM KCl in 75 mM HNO_3 and 75 mM KCl in 25 mM HNO_3, respectively. Because any variation in the amount of scattered radiation is attributable to the change in solution pH, and not to a change in the solution ionic strength or plasma power, these results suggest that acid present in a sample solution contributes to the formation of solution droplets and aerosol ejection. If the same mechanism is responsible for removing analyte from the solution phase and introducing it into the SCGD plasma where it will be excited, the results provide a physical explanation for why

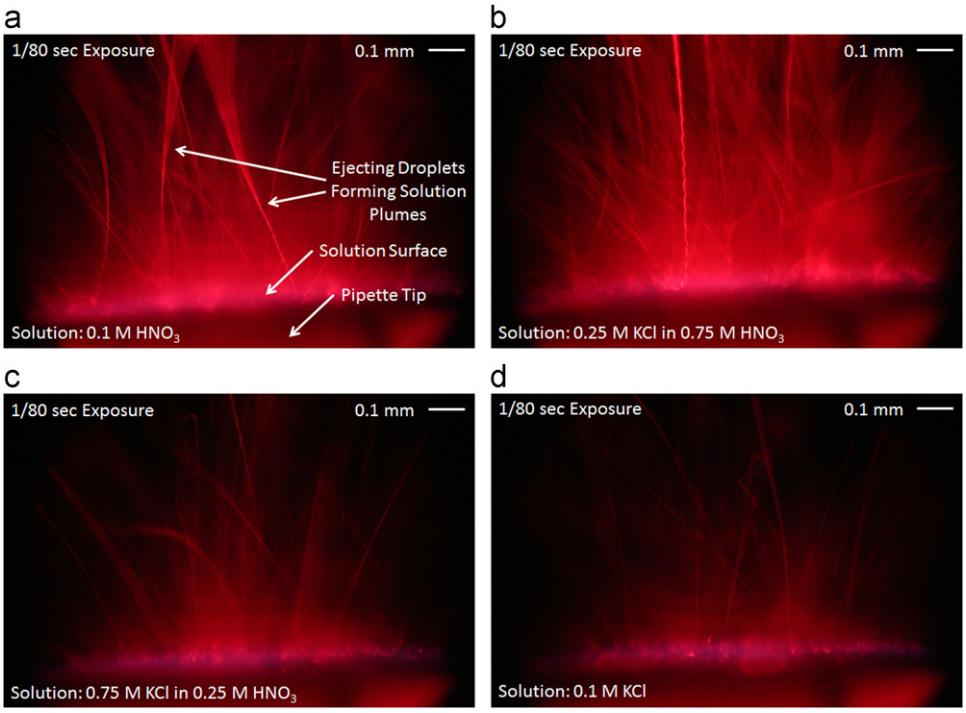

Fig. 3. Laser-scattering images of the SCGD solution–plasma interface. The anode, located 3 mm above the solution surface, is not visible in the images. (a) demonstrates the formation of solution aerosol and droplet plumes, while (b), (c), and (d) demonstrate the effect of changes in acid concentration as ionic strength is held constant.

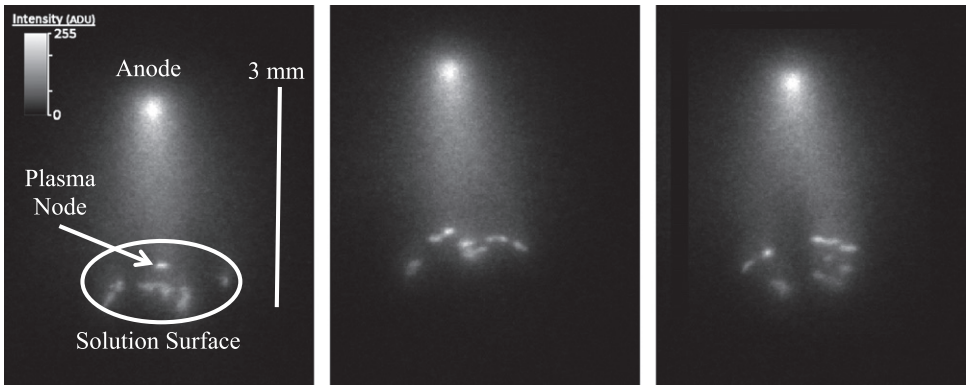

Fig. 4. Representative broadband snapshots of the SCGD with a sample solution of 0.1 M HNO_3 and an ICCD gate duration of 100 μs. The images were not taken in immediate succession, so the observed movement is not representative of the typical motion of emitting nodes over time.

analyte emission from the SCGD drops as the pH of a solution is increased [2,3,7].

3.3. Rapid broadband imaging of the SCGD

In order to study the plasma–solution interface on a faster timescale, broadband-light optical images of the SCGD were collected at framing times of 100 ns–100 μs by use of an ICCD camera. As in experiments described above, a solution of 0.1 M HNO_3 flowing at a rate of 3.2 mL min^{-1} and an applied discharge power of 80 W (1000 V, 80 mA) were used. Three representative images taken at an exposure time of 100 μs and at an angle 30 degrees from the solution surface are displayed in Fig. 4. In Fig. 4(a), the location of the anode and cathodic solution surface are labeled for orientation. Fig. 4(b) and (c) were collected at the same exposure time, however, the images were not collected in immediate succession. The difference in the plasma structure on a fast timescale is immediately evident from a comparison of Fig. 4 with Fig. 3. Longer timescale images show a plasma structure that appears to cover the entire cathode surface. When viewed at fast timescales, however, it becomes evident that the SCGD does not cover the solution surface uniformly, but rather is concentrated in a finite number of plasma 'nodes' upon the solution surface. Further, a comparison of Fig. 4(a) and (c) reveals that these plasma nodes are not stationary, but move to different locations on the solution surface from image to image (i.e. over time). When ICCD exposure times were varied from 100 ns to 100 μs it was found that the total solution surface coverage of the nodes remained constant. When exposure times were lengthened beyond 200 μs, however, the distinct nodal structure was progressively lost due to the motion of the nodes across the liquid surface. The observation of plasma filaments and nodes agrees well with the results of Bruggeman et al., who reported similar structures in glow discharges operated on large, relatively flat water surfaces [11]. These observations suggest that the plasma nodes maintain a consistent structure on the solution surface, but

move across its surface at a rapid rate. Images observed over longer exposure times average this motion to present a homogeneous structure.

The presence of the plasma nodes implies that the power density of the SCGD is likely not uniform across the solution surface, but rather is higher in the localized regions where the plasma forms these nodal structures. The true surface coverage of the nodes was estimated from a series of images and ImageJ (an image-analysis software). The number of nodes at any given time on the surface of an 80 W SCGD with the same 0.1 M HNO_3 solution was found to be approximately 15 ± 4, with each node measuring approximately 50 μm in diameter. The total surface coverage area of the nodes was found to be 0.2 ± 0.03 mm^2, which represents ~15% of the total cathode area. The power density within each of the plasma nodes is then estimated to range from 250 to 500 W mm^{-2}, a value considerably greater than most prior estimates that assumed that the discharge covered the entire solution surface (50 W mm^{-2}). The force applied to the liquid surface due to ion bombardment can then be revisited through Eq. 1. If fifteen equal individual plasma filaments were to carry approximately 7 mA each, the calculated force exerted by each filament would be 0.051 mN. Applied to a spot 50 μm in diameter, the pressure to the surface under each node is estimated to be 3.8×10^3 N m^2. While small in comparison to atmospheric pressure (~10^5 N m^2), this localized ion bombardment force may cause surface deformation. Indeed, Gray and Pharney have shown that a similar effect leads to the creation of particles and droplets in low-current arcs containing plasma filaments [21]. As a plasma node moves from one location on the liquid surface, the recovering force of the surface tension causes a ripple and subsequent formation of a droplet. A similar mechanism may occur in the SCGD, which would explain the node structure and the local increase droplet emission under the same conditions.

The dependence of SCGD structure on solution composition and discharge power was also investigated. Fig. 5 compares images collected with solutions of varying HNO_3 concentration. Solutions of lower acid concentration show a much less pronounced nodal structure, until the nodal structure is almost completely lost at an acid concentration of 0.001 M HNO_3. Considering the effect of lower solution pH on analyte emission and the degree of droplet formation and aerosol generation, these results suggest that node structure, increased droplet formation, and improved analyte emissions could be correlated.

In Fig. 6, the effect of applied power on the structure of the SCGD is shown through a similar set of images. Here, the number of nodes, the coverage area, and the SCGD luminescence all rise with applied power. The plasma node structure does not collapse at higher current, but seems to maintain a consistent current density by addition of more nodes to increase the effective cathode area. These data might also explain why the sensitivity of the source is improved dramatically when sample-introduction capillaries of smaller diameter are used [3,4]; the narrower capillary confines the plasma nodes to a smaller area which increases the probability of nodal emission events being viewable at the monochromator entrance slit, thereby improving analyte emission throughput.

The rapid movement of the nodes across the solution surface demonstrates that the SCGD is not a well-definedspatially homogeneous glow discharge, but rather quite spatially heterogeneous

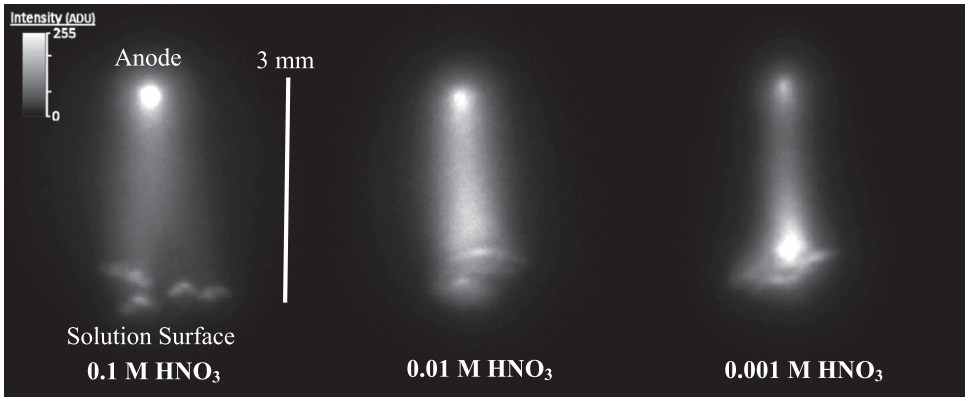

Fig. 5. Effect of electrolyte concentration on the formation of the nodal plasma structure in the SCGD. Images were collected with an ICCD gate duration of 10 μs.

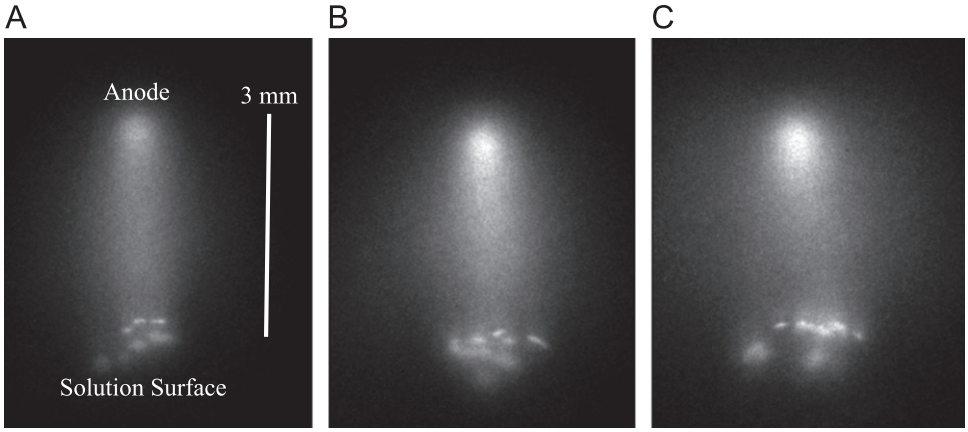

Fig. 6. Effect of applied power on the nodal plasma structure in the SCGD: (A) 60 W (900 V 66 mA), (B) 79 W (1000 V, 79 mA), (C) 100 W (1100 V, 95 mA). Images were collected with an ICCD gate duration of 10 μs.

and dynamic on fast timescales. Thus, the results of previous spectroscopic studies of the SCGD [2–4,11,18,23] represent only the time average of the discharge behavior and not the chaotic nature of the discharge on a fast timescale.

3.4. Rapid monochromatic imaging of the SCGD

The effect of the nodal structure on elemental emission from the SCGD was investigated by employing a rapid monochromatic imaging system. A solution containing 100 ppm NaCl in 0.1 M HNO_3 was introduced into the SCGD and monochromatic images obtained at the sodium atomic emission line at 589.0 nm. These observations were made from a perspective parallel to the solution surface, in contrast to the 30-degree angle used in prior experiments. A series of representative monochromatic images are displayed in Fig. 7, and, as before, each image was collected at the same 100 μs exposure time with none of the images collected in immediate succession. On this short timescale the majority of atomic emission from sodium arises from localized positions on the surface of the solution. These images suggest that the plasma nodes are important contributors to analyte atomization and excitation in the SCGD. Although there appears to be a smaller number of nodes in Fig. 7 than in prior images, the difference is likely due to the perspective from which the images were captured. In Fig. 7, individual nodes likely spatially overlap each other across the surface because of the low angle of observation. Similarly, the apparently homogeneous atomic emission distributed homogenously throughout the negative glow of the SCGD on longer timescales is likely due to the spatial averaging of multiple nodes at variety of locations. Although the specific mechanism of this process cannot be determined from these images alone, the high power density present at the nodes likely contributes to the desolvation and excitation processes.

In order to investigate the effect of solution pH on atomic emission on this rapid timescale, a series of monochromatic images of potassium emission were also obtained. These solutions were identical to those used with the constant ionic strength study performed with the laser-scattering apparatus described earlier. Each of the solutions was imaged at the potassium atomic emission line at 766.5 nm with a constant discharge power of 75 W (1000 V and 75 mA). Two of the images are compared in Fig. 8. These images show that K emission from the SCGD solution surface becomes more sporadic and drops in integrated intensity as the acid concentration in the solution was reduced. At lower acid concentrations, K emission arose predominantly from intermittent explosions of emission from the SCGD solution surface, which were followed by periods of little or no emission. In contrast, solutions containing $\geq$0.025 M HNO_3 displayed more consistent emission from the SCGD solution surface. These images provide further evidence that acidification of sample solutions for use in the SCGD contributes to the solution-to-plasma transport process, perhaps by fostering the nodal plasma structure. Because the plasma covers the entire solution surface at lower acidity (cf. Fig. 7), it can be presumed that the power density is lower in

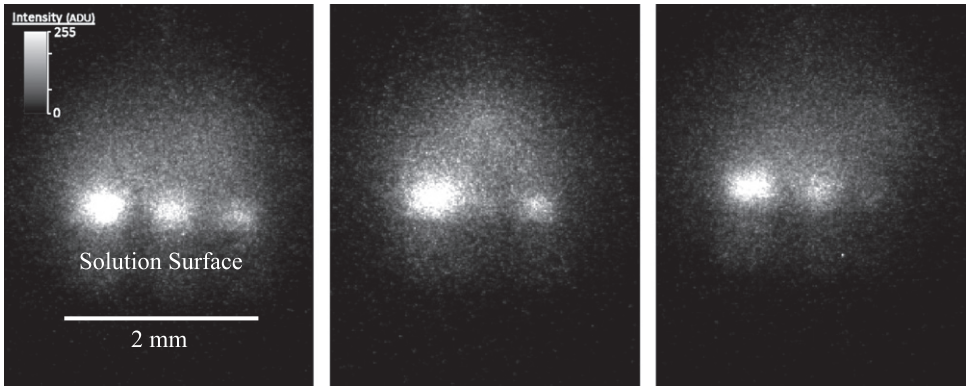

Fig. 7. Monochromatic images of Na 589.0 nm atomic emission from the SCGD during introduction of a solution of 100 ppm NaCl into 0.1 M HNO_3. Images are viewed parallel to the surface of the solution and were collected with an ICCD gate duration of 100 μs.

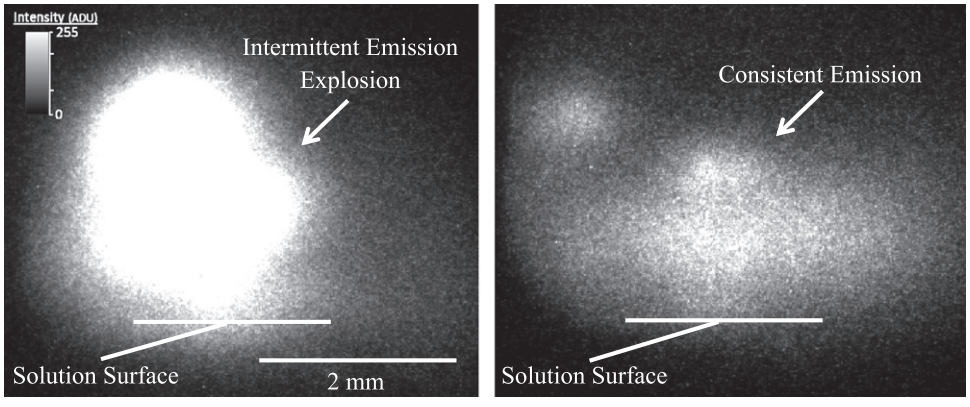

Fig. 8. Monochromatic images of K 766.5 nm atomic emission from two solutions having constant ionic strength of 1.0 but differing concentrations of HNO_3. Images are viewed parallel to the surface of the solution and were collected with an ICCD gate duration of 100 μs.

the solution. This lower power density, in turn, could be reason as to why analyte emission declines in solutions of reduced acidity.

Taken together, these data provide a new view of the operating environment of the analytical SCGD operating with low pH solutions. In contrast to the conventional, relatively static, well-defined glow discharge structure, the SCGD is in fact composed of a number of higher-power plasma nodes that sample analyte solution from various positions along the solution surface on a rapid timescale, and that are responsible for producing most of the atomic emission from analyte solution species. These data also underscore the critical importance of solution pH on SCGD performance. Solution pH, rather than solution conductivity, appears to be an important factor in both the formation of these plasma node structures, as well as the sampling of solution into the SCGD. The reduced presence of solution aerosol and droplets in the discharge at higher pH would result in less analyte transport to the plasma, and thus weaker emission. Further, since the plasma nodes devolve into a structure that covers the entire solution surface at higher pH, the decrease in droplets and aerosol might be attributable to the absence of the nodal structure. Although the detailed mechanisms of these processes cannot be deduced from these observations alone, they provide important insights into the operation of the discharge and form a useful base study from which further experiments regarding the mechanism of the SCGD can be devised.

4. Conclusions

Observations reported here provide new insight into the mechanism of sample solution-to-plasma transport and analyte excitation conditions in the SCGD. High-speed videos of the ignition sequence have shown that the solution surface of the SCGD deforms during ignition and operation, indicating that the solution is altered when the discharge is ignited and operated. Laser-scattering studies and images obtained on a rapid timescale indicate that desolvation also appears to be aided by the presence of acid in solution. Most importantly, nodal plasma structure was observed at 100 ns–100 μs time frames and Na emission was shown to be constrained to the nodal structure, demonstrating that the nodes play a part in atom formation and excitation.

Acknowledgment

Supported in part by the U.S. Department of Energy through Grant DOE DE-FG02-98ER 14890.

Appendix A. Supplementary Information

Supplementary data associated with this article can be found in the online version at http://dx.doi.org/10.1016/j.talanta.2012.07.096.

References

[1] M.R. Webb, G.M. Hieftje, Anal. Chem. 81 (3) (2009) 862–867.
[2] T. Cserfalvi, P. Mezei, P. Apai, J. Phys. D Appl. Phys. 26 (12) (1993) 2184–2188.
[3] M.R. Webb, F.A. Andrade, G. Gamez, R. McCrindle, G.M. Hieftje, J. Anal. At. Spectrom. 20 (2005) 1218–1225.
[4] M.R. Webb, F.J. Andrade, G.M. Hieftje, Anal. Chem. 79 (20) (2007) 7807–7812.
[5] T. Cserfalvi, P. Mezei, Fresenius J. Anal. Chem. 355 (7–8) (1996) 813–819.
[6] T. Cserfalvi, P. Mezei, J. Anal. At. Spectrom. 20 (9) (2005) 939–944.
[7] A.I. Maksimov, V.A. Titov, A.V. Khlyustova, High Energy Chem. 38 (3) (2004) 196–199.
[8] A.I. Maksimov, A.V. Khlyustova, High Energy Chem. 43 (2009) 3149–3155.
[9] T. Suzuki, Y. Matsushima, Y. Mori, T. Yamazaki, T. Noma, J. Mater. Sci. 37 (2002) 595–601.
[10] T. Suzuki, Y. Matsushima, Y. Mori, T. Yamazaki, T. Noma, J. Mater. Sci. 22 (2003) 1259–1260.
[11] P. Bruggeman, J.J. Liu, J. Degroote, M.G. Kong, J. Vierendeels, C. Leys, J. Phys. D Appl. Phys. 41 (2008) 21.
[12] P. Bruggeman, P. Guns, J. Degroote, J. Vierendeels, C. Leys, Plasma Sources Sci. Technol. 17 (2008) 4.
[13] R.K. Marcus, J.A. Broekaert, Glow Discharge Plasmas in Analytical Spectroscopy, Wiley and Sons, West Sussex, 2003.
[14] G.I. Taylor, A.D. Mcewan, J. Fluid Mech. 22 (1965) 1.
[15] J.W. Olesik, G.M. Hieftje, Anal. Chem. 57 (11) (1985) 2049–2055.
[16] P.K. Weissenborn, R.J. Pugh, J. Colloid Interface Sci. 184 (1996) 550–563.
[17] P. Mezei, T. Cserfalvi, L. Csillag, J. Phys. D Appl. Phys. 38 (16) (2005) 2804–2811.
[18] M.R. Webb, G.C.-Y. Chan, F.J. Andrade, G. Gamez, G.M. Hieftje, J. Anal. At. Spectrom. 21 (2006) 525–530.
[19] P. Mezei, T. Cserfalvi, M. Janossy, J. Phys. D Appl. Phys. 31 (11) (1998) L41–L42.
[20] G.I. Taylor, Proc. R. Soc. Ser. A 280 (1382) (1964) 383–397.
[21] E. Gray, J.R. Pharney, J. Appl. Phys. 45 (1974) 667.
[22] A. Gomez, W. Deng, Aerosol Measurements: Principles, Techniques, and Applications, Wiley and Sons, West Sussex, 2011.
[23] M.R. Webb, F.J. Andrade, G.M. Hieftje, J. Anal. Atom. Spectrom. 22 (7) (2007) 766–774.